JACS
JOURNAL OF THE AMERICAN CHEMICAL SOCIETY
pubs.acs.org/JACS
Article

Backbone Hydrogen Bond Energies in Membrane Proteins Are Insensitive to Large Changes in Local Water Concentration

Henry J. Lessen, Ananya Majumdar, and Karen G. Fleming*

Cite This: J. Am. Chem. Soc. 2020, 142, 6227−6235
Read Online

ABSTRACT: A hallmark feature of biological lipid bilayer structure is a depth-dependent polarity gradient largely resulting from the change in water concentration over the angstrom length scale. This gradient is particularly steep as it crosses the membrane interfacial regions where the water concentration drops at least a million-fold along the direction of the bilayer normal. Although local water content is often assumed to be a major determinant of membrane protein stability, the effect of the water-induced polarity gradient upon backbone hydrogen bond strength has not been systematically investigated. We addressed this question by measuring the free energy change for a number of backbone hydrogen bonds in the transmembrane protein OmpW. These values were obtained at 33 backbone amides from hydrogen/deuterium fractionation factors by nuclear magnetic resonance spectroscopy. We surprisingly found that OmpW backbone hydrogen bond energies do not vary over a wide range of water concentrations that are characteristic of the solvation environment in the bilayer interfacial region. We validated the interpretation of our results by determining the hydrodynamic and solvation properties of our OmpW-micelle complex using analytical ultracentrifugation and molecular dynamics simulations. The magnitudes of the backbone hydrogen bond free energy changes in our study are comparable to those observed in water-soluble proteins, the H-segment of the leader peptidase helix used in the von Heijne and White biological scale experiments, and several interfacial peptides. Our results agree with those reported for the transmembrane α-helical portion of the amyloid precursor protein after the latter values were adjusted for kinetic isotope effects. Overall, our work suggests that backbone hydrogen bonds provide modest thermodynamic stability to membrane protein structures and that many amides are unaffected by dehydration within the bilayer.

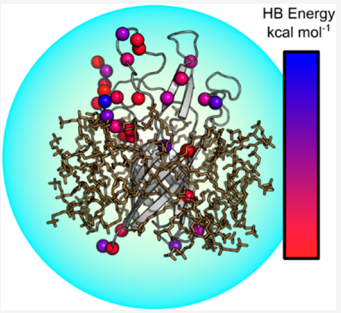

INTRODUCTION

Lipid bilayers provide a unique solvent environment for membrane proteins (MPs) and are essential for the proper folding and function of these biomolecules.[1,2] An improved quantitative understanding of the impact of lipid bilayer structure on MP energetics will boost current design methods[3] and therapeutic development efforts.[4−6] How the bilayer alters MP stability is largely a result of membrane structure, which can be divided into two regions: the hydrocarbon core and the interface.[7] The hydrocarbon core is composed of aliphatic lipid chains,[8] and the interface is a transition region connecting bulk water to the hydrocarbon core.[9] A notable feature of lipid bilayers is the transmembrane (TM) polarity gradient mainly due to depth-dependent changes in hydration levels.[7,10] The water concentration reduces across the interface and reaches a minimum at the hydrocarbon core.[7]

Because the conformation of a protein is intimately related to the chemical nature of its surrounding solvent, the hydration gradient across the interfacial region of the phospholipid bilayer alters the energetics of MP structures. Equilibrium MP folding experiments *in vitro* show that the local water concentration influences the energetic contributions of aromatic side chains in a depth-dependent way.[10] Similarly, partitioning of the leader peptidase α-helical H-segment *in vivo* reveals that side chain residues placed in guest positions along the helix show position-dependent energetics along the bilayer normal in response to the polarity gradient.[11−13] In an independent assay *in vivo*, the stabilizing influences of side chains were inferred from analysis of a library of TM segment variants, which recapitulated bilayer depth-dependent side chain preferences.[14] It is unclear if the protein backbone is affected in the same way.

Due to their electrostatic nature, it is reasonable to assume that backbone hydrogen bonds (bbHBs) would also show a depth dependence in their thermodynamic contributions to MP folds. Consistent with this idea is the fact that reduced water content has been speculated to drive the formation of TM bbHBs.[15] Indeed, a characteristic feature of most MPs is the formation of secondary structure within the membrane-embedded regions, which by definition creates large numbers of bbHBs. Therefore, even small alterations in bbHB stabilities

Received: January 9, 2020
Published: March 5, 2020

https://dx.doi.org/10.1021/jacs.0c00290
J. Am. Chem. Soc. 2020, 142, 6227−6235

due to the bilayer solvation environment could have large energetic consequences for MP stability.[15]

This hypothesis has not been fully tested because methods to directly investigate bbHB energetics are few and technically challenging.[16] However, bbHB energetics can be measured using hydrogen/deuterium fractionation (φ) factors, which report on the equilibrium isotopic preference of individual amides for either protium or deuterium as follows[17−23]

$$\varphi = \frac{[N - D]_{backbone}/[N - H]_{backbone}}{[D]_W/[H]_W} \quad (1)$$

In this definition, $[N - D]_{backbone}$ and $[N - H]_{backbone}$ are the deuterated and protonated populations of a backbone amide, while $[D]_W$ and $[H]_W$ are the concentrations of deuterium and protium in the water. This method minimally perturbs protein structure enabling direct and easily interpretable analysis. An additional advantage is site specificity, because φ factors are collected using nuclear magnetic resonance (NMR) spectroscopy thus providing atomic level resolution. Finally, φ factors can be converted into free energy changes by using an empirical scaling factor to provide quantitative values of bbHB stabilities.[24]

In this study, we measured φ factors for 33 bbHBs in the TM protein OmpW to ask whether reduced water content in the local environment alters any of the bbHB strengths. These amide sites are unambiguously assigned, quantifiable, and completely equilibrated under experimental conditions. The NMR experiments were carried out on OmpW that was reconstituted in sulfobetaine-3-12 (SB3-12) micelles.[25] We used sedimentation velocity (SV) analytical ultracentrifugation (AUC) and molecular dynamics (MD) simulations to demonstrate that the solvation environment of the protein-micelle complex displays a water gradient similar to that observed in bilayer interfaces. We found that the bbHB energies stabilize the folded structure by an average of −1.4 kcal mol^{-1} and are surprisingly constant over a large range of water concentrations. The magnitudes of the OmpW bbHB free energy changes are comparable to those observed in several water-soluble proteins previously obtained using φ factors.[17,20−22] Our values also agree with measurements of average bbHB strength in several interfacial peptides,[26,27] the H-segment of the leader peptidase,[13] and the bbHb energies for the TM α-helical amyloid precursor protein (APP) following adjustment for kinetic isotope effects.[18]

MATERIALS AND METHODS

OMP Expression into Inclusion Bodies (IBs). The plasmid construct and protocol for unlabeled OMP expression and purification has been previously detailed.[28] A brief overview is provided for reference. OmpW lacking the native signal sequence was expressed in HMS *E. coli* cells. All media contained 0.1 mg/mL of ampicillin to select for plasmid containing cells. A 5 mL initial growth was initiated from a glycerol stock stored at −80 °C and grown for 8 to 10 h in LB media at 37 °C. A 50 μL portion of this culture was used to inoculate 25 mL of LB, and this mixture was grown overnight at 37 °C. In the morning, 10 mL of the overnight growth was used to inoculate 500 mL of TB media, and this mixture was grown at 37 °C until it reached an optical density of 1.0 at 600 nm. Protein expression was induced by the addition of isopropyl β-D-1-thiogalactopyranoside (IPTG) to a final concentration of 1 mM. Expressing cells were grown for an additional 5 h and harvested by centrifugation at 5000 rpm for 15 min at 4 °C. The supernatant was discarded, and cell pellets were frozen at −20 °C until IB prep.

Expression of isotopically labeled OmpW was carried out using M9 minimal media(Cold Spring Harbor Protocols[29]) supplemented with different isotopic precursors. For uniform ^{15}N labeling, $^{15}NH_4Cl$ (Cambridge Isotopes: NLM-467) was used. For uniform ^{13}C and ^{2}H labeling, isotopically labeled glucose (Cambridge Isotopes: CDLM-3813) and D_2O (Cambridge Isotopes: DLM-4) were employed. Expression cultures using deuterated glucose used 3 g of isotopically labeled glucose and 1 g of $^{15}NH_4Cl$ per 1 L of D_2O. Protein expression was initiated with a 5 mL starter culture in LB media inoculated from a glycerol stock kept at −80 °C. This was grown for 8 to 10 h at 37 °C. From the starter culture, 3 mL of cells was pelleted and resuspended in 1 mL of M9 media. The resuspended culture was used to inoculate two separate 25 mL growths in M9 media, and these were grown for 16 to 18 h at 37 °C or until the OD_{600} was between 0.8 and 0.9. At this point, the 25 mL growths were each diluted to a final volume of 500 mL. The diluted cultures were grown to an OD_{600} between 0.6 and 0.8, and the cells were induced with 1 mM of IPTG. Cells were allowed to grow for an additional 10 h post induction. The cells were harvested by centrifugation at 5000 rpm for 15 min at 4 °C. The supernatant was discarded, and cell pellets were frozen at −20 °C.

IB Prep. The protocol for purification of OMP IBs has been previously detailed.[10,28] Briefly, each frozen cell pellet from a 500 mL growth was thawed, resuspended in 25 mL lysis buffer (pH 8, 50 mM Tris.HCl, 10 mM EDTA), and lysed using an Avestin EmulsiFlex C3. Brij L23 detergent (Sigma: 9002-92-0) was added to the lysed cell suspension at a final concentration of 0.08% w/v (66 μL for every 25 mL of lysed cells). The cell solution was centrifuged at 4500 rpm for 20 min at 4 °C. The supernatant was discarded, and the IB pellet was resuspended in 25 mL of wash buffer (pH 8, 10 mM Tris.HCl, 1 mM EDTA). This centrifugation procedure was repeated twice. After the final centrifugation step, the IB pellets were frozen at −20 °C.

AUC Sample Prep and SV Experiments. Frozen IB pellets containing OmpW from 500 mL of expression culture were resuspended in 40 mM Tris pH 8 supplemented with 8 M urea (Amresco Ultrapure: 4170833) to create a filtered, stock OmpW concentration ranging between 80 to 100 μM determined by absorbance spectroscopy. This typically involved a resuspension volume of 5 to 25 mL depending on the expression levels of the growth. Resuspended stock was filtered using a 0.45 μm Millex syringe filter, aliquoted into 1 mL samples and frozen at −80 °C until use.

A resuspended OmpW aliquot was thawed and diluted dropwise to a final concentration of 6 μM in 20 mM Tris pH 8, 6.5 mM SB3-12 (Sigma-Aldrich, D0431). The critical micelle concentration for SB3-12 is 2−4 mM,[30] which indicates the presence of micelles under folding conditions. Samples were mixed using a magnetic stir plate and folded for 12 h at 45 °C. After 12 h, the pH of the sample was quickly dropped by adding pH 4 acetate buffer to a final concentration of 40 mM. The solution was equilibrated for 1 h and then filtered using a 0.45 μm Millex syringe filter.

The filtered solution was buffer exchanged by three rounds of concentration and dilution into the final experimental buffer conditions using a 30 kDa spin concentrator (Millipore). The final volume was 500 μL. The final concentrations of SV samples were created by diluting the OmpW stock to 22.8, 17.6, 11.4, or 5.1 μM in a background of 40 mM borate pH 8.0 and 6.5 mM SB3-12.

We used a Beckman XL-I analytical ultracentrifuge to conduct all SV experiments. Samples were loaded into two sector cells and centrifuged at 50000 rpm for 18 h at 20 °C. SV data were collected with an interscan delay of 5 min at 20 °C. Experiments to determine the hydrodynamic properties of the protein micelle complex were conducted in H_2O and were monitored using absorbance at 280 nm using an extinction coefficient of 39420 M^{-1} cm^{-1}. The experiment was repeated a total of 5 times using two independently folded technical replicates (Table S1). Analysis of these SV data was conducted using DCDT+ version 2.4.3.[31,32]

We determined the number of detergent molecules in the protein-micelle complex by collecting SV data using both absorbance and interference optics followed by analysis using Sedfit[33] as previously

https://dx.doi.org/10.1021/jacs.0c00290
J. Am. Chem. Soc. 2020, 142, 6227−6235

described.[34] Only the protein contributes to the absorbance signal at 280 nm, while both detergent and protein contribute to the interference signal. The number of detergents bound was calculated by subtracting the protein contribution to the interference peak from the experimentally observed interference peak for the protein-micelle complex. The refractive increments used to determine weight concentrations were 0.187 and 0.1297 mL g^{-1} for OmpW and SB3-12, respectively. This analysis was repeated 3 times. Table S2 contains additional constants for OmpW and SB3-12; Table S3 shows the results from independent replicas. This number of detergents was used as a guide to construct the MD systems.

MD Simulations. Protein-micelle systems used in MD simulations were built using CHARMM-GUI.[35−38] The starting structure for OmpW was 2MHL.[25] Three separate systems were built with either 55, 60, or 65 SB3-12 detergent molecules. The starting size of the simulation box for each replica was 92 Å x 92 Å x 92 Å, and the systems were neutralized with 150 mM NaCl. Simulations were carried out using NAMD[39] and the CHARMM36 force field.[40] The system was relaxed using the standard CHARMM-GUI micelle relaxation protocol.[36] The system was simulated under isothermal and isobaric conditions (NPT ensemble). The temperature was set to 313.15 K, and pressure was maintained at 1 atm. Temperature was controlled using Nose-Hover thermostat with a 1.0 ps^{-1} damping coefficient, and the bath was not coupled to hydrogen atoms. Constant pressure was maintained using the Langevin piston with a period of 50 fs and decay time of 25 fs. Newton's equations of motion were integrated using 2 fs timesteps, and simulations were run for 300 ns. Hydrogens were constrained using the SHAKE restraint.[41] Root-mean-square deviation of the TM domain was used to monitor convergence of the simulation (Figure S1). Figure S2 shows representative structures of the protein-micelle complex from all three simulations before and after equilibration. Long range electrostatics were evaluated at every integration step using Particle Mesh Ewald method.[42] Short range, nonbonded interactions were determined through a distance cutoff of 12 Å with a smooth switching function applied starting at 10 Å. Nonbonded interactions were evaluated every step and updated every 10 steps.

Hydration and Shape Analysis. HullRad was modified to include SB3-12 detergent atoms in the determination of the convex hull boundaries with the partial specific volume as reported.[43,44] This modified version of HullRad was used to analyze the equilibrated MD trajectory of the protein-micelle complex to determine the sedimentation coefficient from simulation. Figure S3 shows an example of the convex hull computed by HullRad shown on the protein-micelle structure.

The MD trajectories were used to calculate the hydration environment of the protein-micelle complex. The center of mass was set to be a reference for the system and was determined using the TM protein backbone residues and detergent molecules within the micelle. The selection criteria can be found in the SI (*Definition of center of mass selection criteria*). Water was counted within specified distances from the complex center of mass. The number of waters at each radial distance was normalized by the shell volume to obtain the water concentration as a function of radius. This procedure was applied in time steps of 0.2 ns for the final 250 ns of the simulations.

Bilayer and micelle hydration levels were compared using the respective polar atom plane as the reference position (Figure S4). Bilayer hydration data were calculated from previously published simulations of 1,2-dilauroyl-*sn*-glycero-3-phosphocholine (DLPC).[10] We define the polar atom plane in SB3-12 as the average radial position of the quaternary amine nitrogen in the detergent headgroup from the protein-micelle center of mass. The average phosphate position along the bilayer normal for the DLPC membrane. Figure S4 shows a cartoon schematic of the polar atom plane for both the micelle and protein system. Using this reference state, negative distances indicate atoms closer to the center of the TM regions and positive values indicate more soluble regions.

NMR Sample Prep. NMR samples were folded and concentrated using the same procedure described above for the AUC samples. Final sample conditions after buffer exchange were 40 mM borate pH 8.0, 180 mM SB3-12. Samples used for backbone assignments contained 670 μM OmpW and 10% D_2O in a volume of 400 μL. φ factor samples all contained 250 μM OmpW and varying amounts of D_2O. A total of 8 samples were prepared with the following D_2O volume fractions: 0.25, 0.3, 0.35, 0.4, 0.45, 0.5, 0.55, 0.65, 0.70, and 0.75. Three separate samples containing equal amounts of H_2O and D_2O were prepared to assess the total error of the samples.

NMR Assignments. Initial backbone assignments were obtained by mapping over assignments previously published (BMRB Entry: 19637).[25] The mapped assignments were confirmed by collecting transverse-relaxation optimized spectroscopy (TROSY) versions of 3D HNCα, HNCαCβ, and HN(C′)Cα experiments collected on a Bruker Avance III 800 MHz spectrometer equipped with a CPQCI cryoprobe. Data were acquired using nonuniform sampling (NUS) in both indirect dimensions. NUS-TROSY pulse sequences employing coherence selection via pulse field gradients were coded in-house using Topspin 2.1. Sampling schedules were generated using the Poisson Gap schedule generator[45] and were sampled at 15%. The SI contains additional details regarding the specific parameters and pulse sequences of the experiments. Reconstruction of NUS data was carried out using NESTA and NMRPipe.[46,47] NMRPipe was used to process reconstructed data. Cara was used to assign and visualize spectra.[48] Table S4 lists final assignments.

NMR φ Factor Equilibration. We ensured sample equilibration for φ factor determinations using both kinetic and end point analysis. We determined approximate equilibration times by measuring hydrogen to deuterium exchange kinetic rates of OmpW as described in detail in the SI and as shown in Figures S5, S6, and Table S5. We calculated the sample equilibration time to equal 5 times the inverse of the slowest measurable exchange rate.

To ensure that the experimental system reached complete equilibrium, we additionally performed end point analysis by comparing the peak heights from two independent samples in which one was folded and prepared in D_2O and the other was folded and prepared in H_2O, and both were diluted to a final H_2O/D_2O (v:v) ratio equal to 1.0. Samples used in this experiment were ^{15}N labeled and contained 200 μM OmpW in 40 mM borate at pH 8.0 with 180 mM SB3-12 detergent. Samples were equilibrated at 40 °C using a benchtop incubator for 5 weeks. The $^1H-^{15}N$ 2D TROSY experiments were collected on a 600 MHz Bruker AVANCE II spectrometer equipped with a TCI cryoprobe. Parameters for individual acquisitions were 64 scans per FID, interscan delay of 2.5 s, direct acquisition time of 60 ms, and 50 ms in the indirect dimension. We normalized absolute signal differences between the samples using a long-range $^1H-^{15}N$ HSQC for histidine rings that correlates *nonexchangeable* aromatic H−C protons with histidine ring ^{15}N nuclei via two bond ($^2J_{NH}$) couplings.[49] Parameters for each experiment were as follows: 256 scans per FID, acquisition time of 60 ms in the direct dimension, interscan delay of 1.5 s, and 10 ms in the indirect dimension. Spectra were collected at 40 °C, and the positions of the reference peaks were 6.50 ^1H δ (ppm) and 164.5 ^{15}N δ (PPM).

Amide exchange kinetics are not directly related to bbHB strength in φ factor experiments. The φ factor is an *equilibrium* effect, and, therefore, the system must establish complete equilibration to enable accurate analysis. The TM residues most centrally located in the protein-micelle complex did not exchange (even after 5 months). It is tempting to interpret these data as being reflective of excessive bbHB strength, but in reality, it shows only the inability of the solvent environment to catalyze HDX in the accessible time frame. Traditional HDX experiments usually highlight residues that are coupled to the global unfolding of the protein and are slow exchanging.[50] These very slow exchanging residues are most likely reflecting the global unfolding of OmpW and not the dynamics of individual or local bbHB formation. bbHB strength has been shown to relate to isotopic preference of the amide with respect to solvent composition,[51] which can only be interpreted at sites that equilibrate with respect to the solvent. Sites that do not fully equilibrate do not reflect this isotopic preference and, therefore, provide no insight into bbHB strength using the method described in this study.

https://dx.doi.org/10.1021/jacs.0c00290
J. Am. Chem. Soc. 2020, 142, 6227−6235

Data Collection and Analysis for φ Factor Determination. NMR experiments were conducted at 40 °C. Outside of the spectrometer, samples were equilibrated at 40 °C using a benchtop incubator. TROSY experiments used to determine φ factors were collected on an Agilent Inova 800 MHz spectrometer with room temperature triple resonance probe optimized for ^{1}H detection. Table S6 lists data acquisition parameters employed.

Spectra were processed using NMRPipe and further analyzed using Sparky.[52] Peak volumes were fit using a 3D Gaussian function, and the baseline noise level was assessed using a random sampling of 10000 points from the spectrum. To ensure that the peak volumes accurately reflect the protonated population, only fits resulting in RMSD values less than 25% were used to determine φ factors.

We determined values for φ factors using eq 2[22] implemented in R Studio

$$\frac{1}{y} = C\left[\varphi\left(\frac{1-x}{x}\right) + 1\right] \tag{2}$$

where y is the peak volume, x is the volume fraction of H_2O, C is a normalization constant, and φ is the φ factor as defined earlier. The data were fit using weighted least-squares linear regression where the weights for individual points equaled the squared inverse of the peak volume fit RMSD as reported by Sparky. The φ factors were determined by dividing the slope of the fitted relationship by the intercept. The error of the fit was used as the φ factor error. φ factor values were not reported for with R^2 values less than 0.7. Table S7 shows fit results.

Because the empirical scale was developed at 25 °C, φ factors were temperature corrected using the scaling described[24] and are reported in Table S7. The adjusted φ factor values were converted into bbHB energies using the empirically derived relationship[24]

$$\Delta G_{HB} = 7.0^{*}RT\ln\varphi \tag{3}$$

where R is the ideal gas constant, T is the temperature, ΔG_{HB} is the bbHB free energy change, and φ is the φ factor.

We define all bbHB energies in folded proteins to use the random coil amide as a reference state. The φ factor of a random coil peptide is 1.1,[21] which corresponds to a reference energy of +0.4 kcal mol^{-1} when evaluated using eq 3. The bbHb energy for a random coil is subtracted from all bbHB energies determined using the Cao and Bowie scale.

Estimation of Kinetic Isotope Effects in APP φ Factors. The φ factors reported for APP were determined *indirectly* by measuring kinetic rates for hydrogen-to-deuterium exchange ($k_{ex,\,H\to D}$) and conversely deuterium-to-hydrogen exchange ($k_{ex,\,D\to H}$).[18] Mathematically, the φ factor is defined as

$$\varphi_{APP} = \frac{k_{ex,H\to D}}{k_{ex,D\to H}} \tag{4}$$

so that φ_{APP} is the φ factor reported by Bowie and colleagues in APP.[18] This differs from the method employed in this work, which *directly* observes the protonated amide species through 3D peak volumes collected in the ^{1}H−^{15}N 2D TROSY experiment. Although the indirect approach can in principle be used, a known confounding factor is that kinetic exchange rates are influenced by experimental pH[50] and kinetic isotope effects[53] in addition to bbHB strength.

Kinetic isotope effects should be observable in exchange rates measured in EX2 conditions, which were reported in the APP experiments.[18] Under EX2 conditions, the amide exchange rates are defined as follows

$$k_{ex} \approx (P.\,F.\,)k_{\mathrm{int}} \tag{5}$$

where *P.F.* is the protection factor and k_{int} is the intrinsic amide exchange rate constant. It is well-known that strong kinetic isotope effects alter the magnitude of k_{int} depending on the isotopic composition of the exchange buffer.[53] Using the SPHERE server,[54] we calculated the k_{int} values for the H → D and D → H reactions for APP backbones under the experimental conditions reported in Cao et al.[18] Taking the ratio of these intrinsic rate constants (similar to eq 4), a position dependent term is obtained (Table S8). This term reflects differences in the exchange kinetics of a *non-hydrogen bonded* amide due to solvent isotope content and *does not* inform on equilibrium bbHB strength. Therefore, the previously reported φ factors and bbHB strengths were adjusted accordingly. APP bbHB energies reported in Table S9 also include the adjustment made for the random coil amide reference state mentioned previously in this work.

RESULTS

Steep Water Gradient Across a Bilayer Interface Is Approximated by the OmpW-Micelle System. A hallmark chemical property of the biological lipid bilayer is the steep polarity gradient found in the interface between bulk water and the hydrophobic center. This changing solvent environment is expected to influence energetic interactions important for stabilizing MP structures. In this investigation of OmpW bbHBs energies, we first validate that our micellar system mimics this characteristic interfacial property.

We used a combination of SV, MD simulations, and hydrodynamic modeling to build experimentally derived atomic models of the OmpW-micelle particle representative of the sample used for bbHB energy determination. Figure 1A shows a snapshot of the equilibrated OmpW-micelle structure. Figure 1B shows the sedimentation coefficient distribution revealing a weight-average sedimentation coefficient of the complex equal to 1.93 ± 0.088 S. This distribution informs on the size, shape, and number of detergents bound. Figure S7 shows a c(s) distribution of a sample in which both absorbance and interference optics were used simultaneously to measure the sedimentation profile from which the value of 59 ± 2 bound detergent molecules was determined. HullRad hydrodynamic prediction across all equilibrated trajectories reports an average value of 1.94 ± 0.02 S. The excellent agreement between experimental and predicted hydrodynamic parameters validates the usage of the OmpW-micelle MD models for hydration gradient analysis.

Figure 1C shows the average water gradient from the combined 750 ns over the three independent MD trajectories. This gradient shows a steeply declining water concentration across the depth of the micelle from bulk solvent to the surface of OmpW. Figure 1C further shows that the water decline is similar to that found in lipid bilayers.[10] The sites of measured φ factors are shown overlaid on the OmpW-micelle water gradient, where it can be observed that we were able to measure bbHB strengths over a wide range of water concentrations.

bbHB Energies Stabilize Folded OmpW. Our measurements of bbHB free energies in OmpW indicate an overall preference for the folded state. Figure 2 shows that our H/D exchange has reached equilibration as early as the five-week time point and is independent of starting conditions. Figure 3A shows that the majority of measured φ factors are less than one, indicating a preference of protium relative to deuterium in OmpW. Figure S11 shows representative spectra demonstrating no significant changes were observed in the ^{1}H−^{15}N TROSY-HSQC spectra during equilibration, indicating that the protein remained fully folded during the duration of the experiment.

Figure 3B presents the corresponding Gibbs free energy change for bbHB formation upon folding calculated from the φ factors using the Cao and Bowie scaling factor.[24] The average bbHB strength measured in OmpW was −1.4 ± 1.2 kcal

https://dx.doi.org/10.1021/jacs.0c00290
J. Am. Chem. Soc. 2020, 142, 6227−6235

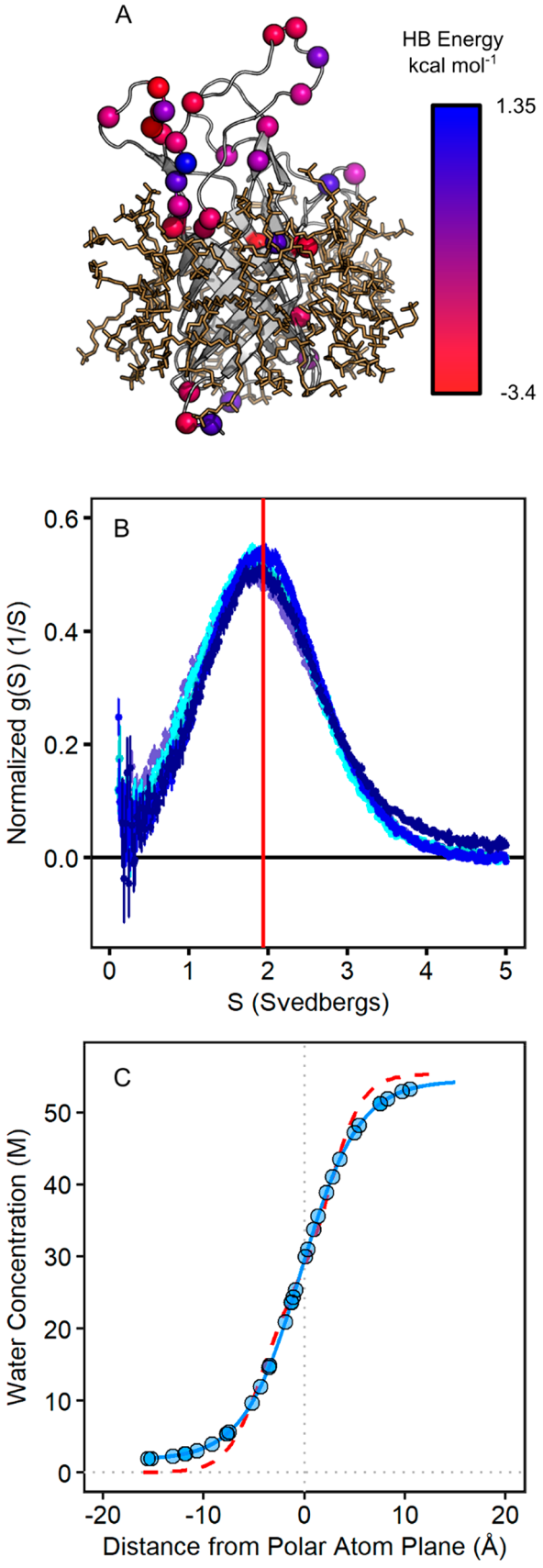

Figure 1. Simulations recapitulate experimental hydrodynamic properties of the protein-micelle complex. (A) Snapshot of OmpW-micelle complex with 59 bound detergent molecules. This snapshot was from the build with 60 detergents. HullRad predicts a sedimentation coefficient of 1.95 for this snapshot. (B) Overlay of normalized g(S) distributions from five independent experiments is shown in different shades of blue. These yield an average sedimentation coefficient of 1.93 ± 0.088 S. The sedimentation coefficient calculated from all MD trajectories is overlaid as a red line (1.94 ± 0.02 S). Error bars on points of individual normalized g(S) curves correspond to standard deviations for those points. Table S1 shows values obtained for each SV experiment. Figure S8 shows the distributions summarizing the results of the HullRad analysis for all simulations. (C) Water gradients calculated from OmpW-micelle (blue line) and DLPC (red dashed line). Overlaid points are calculated water concentrations for OmpW amides whose φ factors were measured. Figure S9 and Tables S10 and S11 report the fit parameters for these gradients. Figure S10 shows the radial distributions of the other polar atom groups and acyl chain carbons in the protein-micelle complex for reference.

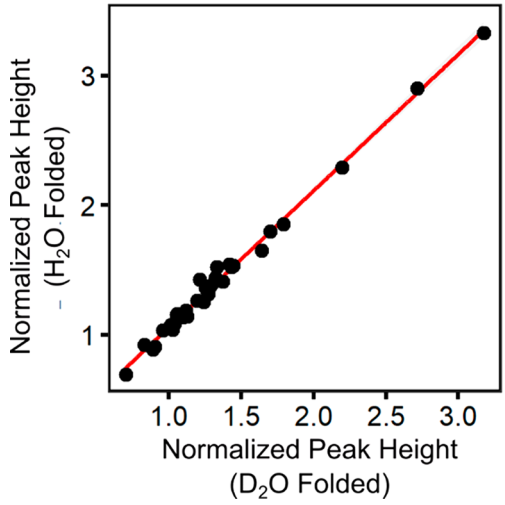

Figure 2. Measured φ factors are at equilibrium. Samples prepared in H_2O or D_2O show the same normalized peak height when diluted to 1:1 H_2O/D_2O and equilibrated for 5 weeks at 40 °C. Fit line (red) shows a slope of 1.05 ± 0.02 with an R^2 of 0.99 and indicates that two samples have reached pathway-independent equilibrium.

mol^{-1}. The reference state for these free energy changes is the random coil, aqueous state, and, therefore, the majority of amides investigated indicate a preference for the folded state.

bbHBs Energies Do Not Vary Across the Polarity Gradient. As shown in Figure 1C, the reported residues sample a multitude of local solvation environments. Figure 4 shows that bbHB stabilities measured in OmpW do not correlate with local water content. We also observe no dependence of bbHB energies on local water orientation (Figure S13).[55] To further test for differences in bbHB energies in different regions of the protein, we subdivided the OmpW sites into *Interfacial* and *Soluble* bbHBs. *Interfacial* bbHBs were located below the polar atom plane (closer to protein-micelle center), and soluble bbHBs were located above that plane. Table S12 shows that these two groups show no significant differences.

We compared the *Soluble* and *Interfacial* groups on OmpW to distributions for other bbHB free energies determined using φ factors. Figure 5 shows that average bbHB strength in OmpW is similar to values observed in water-soluble proteins. The similarities in these distributions agree with our finding that bbHB strength is independent of local water concen-

https://dx.doi.org/10.1021/jacs.0c00290
J. Am. Chem. Soc. 2020, 142, 6227−6235

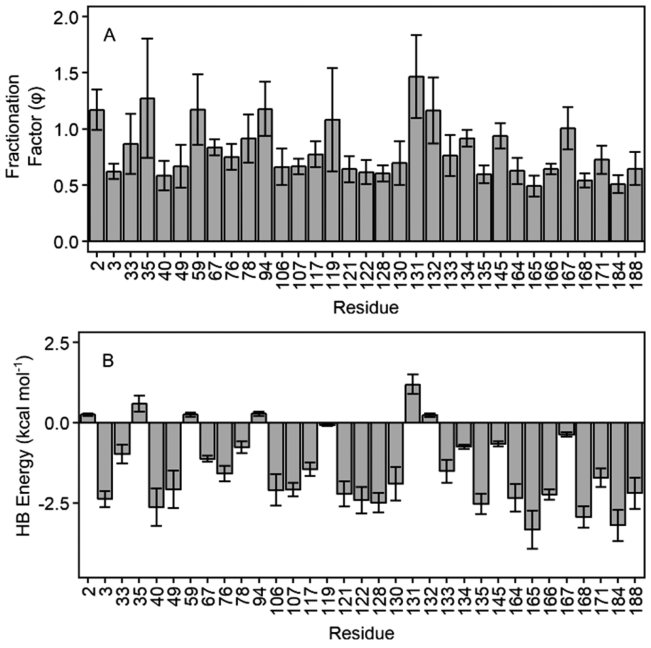

Figure 3. Backbone hydrogen bond energies in OmpW favor the folded state. (A) Values for φ factors from 33 backbone amide sites on OmpW. The majority of backbone amides investigated prefer protium relative to deuterium ($\varphi < 1$). (B) Negative bbHB energies for backbone amides indicate a preference for the folded state (see Figure S12 for a fitting example).

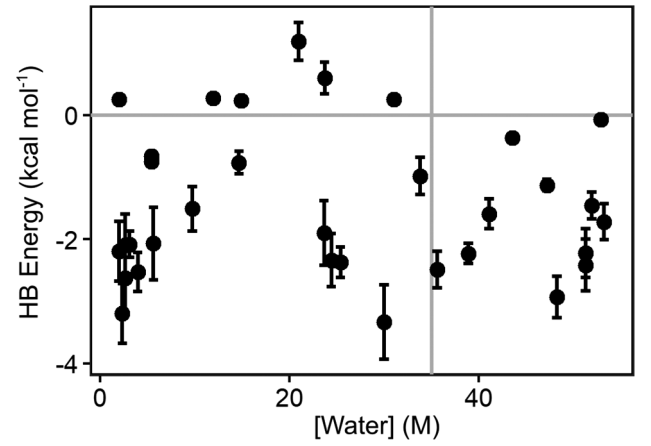

Figure 4. bbHB energy does not correlate with water concentration. Water concentration for individual amide sites was calculated using the relationship determined from MD simulations. Energies are uniformly distributed across the concentration range investigated and show no significant correlation.

tration. Further, our direct measurements of bbHB free energies are comparable with previous estimates of the contribution of interfacial bbHBs to folding of peptides at the interfacial surfaces of phospholipid bilayers (−0.5 to −0.6 kcal mol^{-1} for both α-helices and β-sheets)[27,56] and with estimates of bbHB strengths of the α-helical H-segment *in vivo* (an apparent free energy of −0.7 kcal mol^{-1}).[13] The agreement between HB strength in water-soluble proteins, interfacial peptide folding, *in vivo* estimates from von Heijne biological measurements, and OmpW implies the general conclusion that bbHB energetics do not vary substantially between interfacial and aqueous folding environments, which supports the finding

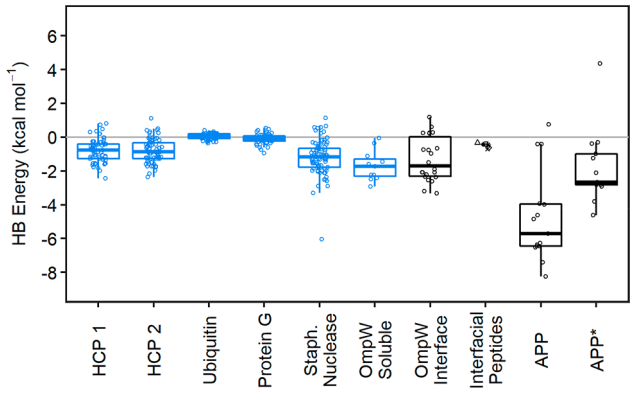

Figure 5. Interfacial and soluble bbHB energies in OmpW are similar to bbHB energies in water-soluble proteins. Distributions of bbHB energies are shown as points with a box plot of the distribution overlaid (black showing interfacial measurements and blue showing water-soluble proteins and OmpW loops). Water-soluble protein bbHB averages were obtained from previous φ factor studies of two different histidine containing proteins (HCP1 and HCP2),[17] ubiquitin,[21] and Protein G[20] staphylococcal nuclease,[22] soluble regions of OmpW, interfacial regions of OmpW, measurements from interfacial peptides, APP as originally reported,[18] and APP values adjusted for kinetic isotope effects (APP*). APP is a single pass α-helical MP solubilized in a LMPG detergent micelle. Interfacial peptide energy symbols are as follows: β-strand forming peptide on 1-palmitoyl-2-oleoyl-*sn*-glycero-3-phosphocholine (◇) and 1-oleoyl-2-(9,10-dibromostearoyl)-*sn*-glycero-3-phosphocholine (*),[56] two peptides that have an α-helical structure within the interface (AQL △, TP10 ●),[27] the interfacial α-helix melittin (□).[26] The bbHB strength inferred from the biological scale is also plotted in this group (×).[13] All φ factors were temperature corrected to 298.15 K before being converted into free energies using the Cao and Bowie method.[24]

that bbHBs are generally insensitive to local solvent environment over a wide range of water concentrations.

The bbHB strengths previously reported for the APP α-helix represent a potential exception to the generality of our findings, because the bbHB energies appear to be much more favorable in this protein. Given the environmental invariance we observe across bilayers, micelles, and bulk water, we do not expect the solvation in the 1-myristoyl-2-hydroxy-*sn*-glycero-3-phospho-(1′-rac-glycerol) (LMPG) micelles employed in that study to be significantly different. Still, the average bbHB energy in APP[18] were reported to be 3.4 kcal mol^{-1} more favorable as compared to OmpW. We postulated that this discrepancy may reflect methodological differences. Using the ratio of the k_{int} rates of the H → D and D → H reactions (Table S8), the reported bbHB stabilities for APP were adjusted to account for kinetic isotope effects. Our analysis reveals that the initial measurements of APP bbHB stabilities become on average 3.61 kcal mol^{-1} less favorable (APP* in Figure 5, Table S9) and are thus directly comparable to all other known values.

DISCUSSION

The insensitivity of bbHB strengths to local water concentrations has important implications for understanding both interfacial and TM protein structures and functions. At interfacial regions of the membrane, bbHB formation as a basis of secondary structure stabilization is still favorable because of the higher energy observed for the non-hydrogen bonded peptide bond.[15] Yet, it would appear to be *not significantly more stable* than it would otherwise be in water. A

https://dx.doi.org/10.1021/jacs.0c00290
J. Am. Chem. Soc. 2020, 142, 6227−6235

caveat to a more general conclusion concerns the most dehydrated regions of the bilayer. The minimum water concentration in our OmpW-micellar system is 2 M, and our study cannot draw conclusions about bbHB energies in lower water concentrations. Even so, we are able to access bbHB energies over a steep water gradient that is characteristic of the bilayer interface. This means that secondary structures in regions of large MPs, such as transporters that undergo changes in hydration as part of their functional cycles, will have their conformations and dynamics modulated more by changes in side chain solvation as compared to differences in hydrogen bond strengths.

Similarly, our results imply that secondary structure regions of MPs lining aqueous vestibules of ion channels are unlikely to be less stable than similar α-helical segments that are membrane-embedded. Our data also show that bbHBs exposed to interfacial concentrations of water are less costly to break than previously assumed. The implications of this finding are particularly important for several essential TM β-barrels, including BamA and LptD, which are proposed to function using a "lateral gate mechanism" in which bbHBs break between the first and last β-strands.[57] The solvated barrel lumen and small number of bbHBs observed at these β-strand interfaces in crystal structures of these proteins[58−60] suggest that the energetic penalty of lateral gate opening is not as costly as was previously speculated.[61]

CONCLUSION

In summary, our work clarifies the role of local water concentration on bbHB strength. Our results demonstrate that bbHBs located in regions that approximate the bilayer interface contribute a modest −1.4 kcal mol^{-1} per peptide backbone to MP stability. Remarkably, the stabilities of these bonds are insensitive to a large range of water concentrations. Our findings agree with previous measurements of bbHBs from a multitude of systems including interfacial peptides with both α-helical and β-sheet structures, estimates from the biological scale, corrected values for the transmembrane α-helix APP, and with soluble proteins. The agreement between such a vast number of systems suggests that our measurements reflect a general trend in bbHB energetics over the many levels of hydration. Overall, our study unifies the role of bbHBs in protein stability across multiple environments, allowing for a more complete understanding of the protein folding problem.

ASSOCIATED CONTENT

Supporting Information

The Supporting Information is available free of charge at https://pubs.acs.org/doi/10.1021/jacs.0c00290.

HDX exchange experiments, MD atom selection, statistical testing of bbHB distributions, and water orientation analysis; additional results including relaxation of OmpW in simulations, AUC experimental details, example NMR spectra, HDX derived equilibration times, NMR chemical shifts, NMR experimental parameters, fitting information, correction of APP HB energies for kinetic isotope effects, and water orientation analysis (PDF)

AUTHOR INFORMATION

Corresponding Author

Karen G. Fleming − *T.C. Jenkins Department of Biophysics, Johns Hopkins University, Baltimore, Maryland 21218, United States;* orcid.org/0000-0001-5417-8830; Email: Karen.Fleming@jhu.edu

Authors

Henry J. Lessen − *T.C. Jenkins Department of Biophysics, Johns Hopkins University, Baltimore, Maryland 21218, United States*

Ananya Majumdar − *The Johns Hopkins University Biomolecular NMR Center, Johns Hopkins University, Baltimore, Maryland 21218, United States*

Complete contact information is available at: https://pubs.acs.org/10.1021/jacs.0c00290

Funding

The work was funded by the following sources: N.I.H Grants: R01 GM079440 (K.G.F.) and T32 GM008403, XSEDE Grant: MCB120050

Notes

The authors declare no competing financial interest.

ACKNOWLEDGMENTS

This work would like to acknowledge facilities provided by the Johns Hopkins University Biophysical NMR Center, the Johns Hopkins University Center for Molecular Biophysics, and the University of Maryland College Park Biomolecular NMR Center. This research project was conducted in part using computational resources at the Maryland Advanced Research Computing Center (MARCC). This work used the Extreme Science and Engineering Discovery Environment (XSEDE)[62] under award number NSF MCB120050, which is supported by NSF grant number ACI-1548562. The authors would also like to thank the other members of the Fleming lab for helpful discussion and input on the manuscript.

ABBREVIATIONS

bbHB, backbone hydrogen bond; NMR, nuclear magnetic resonance; MP, membrane proteins; φ factor, hydrogen/deuterium fractionation factor; TM, transmembrane; AUC, analytical ultracentrifugation; MD, molecular dynamics; OmpW, outer membrane protein W; SB3-12, sulfobetaine-3-12; IB, inclusion body; SV, sedimentation velocity; HDX, hydrogen/deuterium exchange; APP, amyloid precursor protein; DLPC, 1,2-dilauroyl-*sn*-glycero-3-phosphocholine; TROSY, transverse-relaxation optimized spectroscopy

REFERENCES

(1) Andersen, O. S.; Koeppe, R. E., 2nd Bilayer thickness and membrane protein function: an energetic perspective. *Annu. Rev. Biophys. Biomol. Struct.* **2007**, *36*, 107−30.

(2) Phillips, R.; Ursell, T.; Wiggins, P.; Sens, P. Emerging roles for lipids in shaping membrane-protein function. *Nature* **2009**, *459* (7245), 379−85.

(3) Kroncke, B. M.; Duran, A. M.; Mendenhall, J. L.; Meiler, J.; Blume, J. D.; Sanders, C. R. Documentation of an Imperative To Improve Methods for Predicting Membrane Protein Stability. *Biochemistry* **2016**, *55* (36), 5002−9.

(4) International Transporter, C.; Giacomini, K. M.; Huang, S. M.; Tweedie, D. J.; Benet, L. Z.; Brouwer, K. L.; Chu, X.; Dahlin, A.; Evers, R.; Fischer, V.; Hillgren, K. M.; Hoffmaster, K. A.; Ishikawa, T.; Keppler, D.; Kim, R. B.; Lee, C. A.; Niemi, M.; Polli, J. W.; Sugiyama,

Y.; Swaan, P. W.; Ware, J. A.; Wright, S. H.; Yee, S. W.; Zamek-Gliszczynski, M. J.; Zhang, L. Membrane transporters in drug development. *Nat. Rev. Drug. Discovery* **2010**, *9* (3), 215−36.
(5) Marinko, J. T.; Huang, H.; Penn, W. D.; Capra, J. A.; Schlebach, J. P.; Sanders, C. R. Folding and Misfolding of Human Membrane Proteins in Health and Disease: From Single Molecules to Cellular Proteostasis. *Chem. Rev.* **2019**, *119* (9), 5537−5606.
(6) Overington, J. P.; Al-Lazikani, B.; Hopkins, A. L. How many drug targets are there? *Nat. Rev. Drug Discovery* **2006**, *5* (12), 993−6.
(7) Nagle, J. F.; Tristram-Nagle, S. Structure of lipid bilayers. *Biochim. Biophys. Acta, Rev. Biomembr.* **2000**, *1469* (3), 159−95.
(8) Mathai, J. C.; Tristram-Nagle, S.; Nagle, J. F.; Zeidel, M. L. Structural determinants of water permeability through the lipid membrane. *J. Gen. Physiol.* **2008**, *131* (1), 69−76.
(9) White, S. H.; Wimley, W. C. Hydrophobic interactions of peptides with membrane interfaces. *Biochim. Biophys. Acta, Rev. Biomembr.* **1998**, *1376* (3), 339−52.
(10) McDonald, S. K.; Fleming, K. G. Aromatic Side Chain Water-to-Lipid Transfer Free Energies Show a Depth Dependence across the Membrane Normal. *J. Am. Chem. Soc.* **2016**, *138* (25), 7946−50.
(11) Hessa, T.; Kim, H.; Bihlmaier, K.; Lundin, C.; Boekel, J.; Andersson, H.; Nilsson, I.; White, S. H.; von Heijne, G. Recognition of transmembrane helices by the endoplasmic reticulum translocon. *Nature* **2005**, *433* (7024), 377−81.
(12) Hessa, T.; Meindl-Beinker, N. M.; Bernsel, A.; Kim, H.; Sato, Y.; Lerch-Bader, M.; Nilsson, I.; White, S. H.; von Heijne, G. Molecular code for transmembrane-helix recognition by the Sec61 translocon. *Nature* **2007**, *450* (7172), 1026−30.
(13) Ojemalm, K.; Higuchi, T.; Lara, P.; Lindahl, E.; Suga, H.; von Heijne, G. Energetics of side-chain snorkeling in transmembrane helices probed by nonproteinogenic amino acids. *Proc. Natl. Acad. Sci. U. S. A.* **2016**, *113* (38), 10559−64.
(14) Elazar, A.; Weinstein, J.; Biran, I.; Fridman, Y.; Bibi, E.; Fleishman, S. J., Mutational scanning reveals the determinants of protein insertion and association energetics in the plasma membrane. *eLife* **2016**, *5*. DOI: 10.7554/eLife.12125
(15) White, S. H.; Wimley, W. C. Membrane protein folding and stability: physical principles. *Annu. Rev. Biophys. Biomol. Struct.* **1999**, *28*, 319−65.
(16) Gao, J.; Bosco, D. A.; Powers, E. T.; Kelly, J. W. Localized thermodynamic coupling between hydrogen bonding and micro-environment polarity substantially stabilizes proteins. *Nat. Struct. Mol. Biol.* **2009**, *16* (7), 684−90.
(17) Bowers, P. M.; Klevit, R. E. Hydrogen bonding and equilibrium isotope enrichment in histidine-containing proteins. *Nat. Struct. Mol. Biol.* **1996**, *3* (6), 522−31.
(18) Cao, Z.; Hutchison, J. M.; Sanders, C. R.; Bowie, J. U. Backbone Hydrogen Bond Strengths Can Vary Widely in Transmembrane Helices. *J. Am. Chem. Soc.* **2017**, *139* (31), 10742−10749.
(19) Jarret, R. M.; Saunders, M. A new method for obtaining isotopic fractionation data at multiple sites in rapidly exchanging systems. *J. Am. Chem. Soc.* **1985**, *107* (9), 2648−2654.
(20) Khare, D.; Alexander, P.; Orban, J. Hydrogen bonding and equilibrium protium-deuterium fractionation factors in the immunoglobulin G binding domain of protein G. *Biochemistry* **1999**, *38* (13), 3918−25.
(21) LiWang, A. C.; Bax, A. Equilibrium Protium/Deuterium Fractionation of Backbone Amides in U−13C/15N Labeled Human Ubiquitin by Triple Resonance NMR. *J. Am. Chem. Soc.* **1996**, *118* (50), 12864−12865.
(22) Loh, S. N.; Markley, J. L. Hydrogen bonding in proteins as studied by amide hydrogen D/H fractionation factors: application to staphylococcal nuclease. *Biochemistry* **1994**, *33* (4), 1029−36.
(23) Shi, Z.; Krantz, B. A.; Kallenbach, N.; Sosnick, T. R. Contribution of hydrogen bonding to protein stability estimated from isotope effects. *Biochemistry* **2002**, *41* (7), 2120−9.
(24) Cao, Z.; Bowie, J. U. An energetic scale for equilibrium H/D fractionation factors illuminates hydrogen bond free energies in proteins. *Protein Sci.* **2014**, *23* (5), 566−75.
(25) Horst, R.; Stanczak, P.; Wuthrich, K. NMR polypeptide backbone conformation of the E. coli outer membrane protein W. *Structure* **2014**, *22* (8), 1204−1209.
(26) Ladokhin, A. S.; White, S. H. Folding of amphipathic alpha-helices on membranes: energetics of helix formation by melittin. *J. Mol. Biol.* **1999**, *285* (4), 1363−9.
(27) Almeida, P. F.; Ladokhin, A. S.; White, S. H. Hydrogen-bond energetics drive helix formation in membrane interfaces. *Biochim. Biophys. Acta, Biomembr.* **2012**, *1818* (2), 178−82.
(28) Burgess, N. K.; Dao, T. P.; Stanley, A. M.; Fleming, K. G. Beta-barrel proteins that reside in the Escherichia coli outer membrane in vivo demonstrate varied folding behavior in vitro. *J. Biol. Chem.* **2008**, *283* (39), 26748−58.
(29) M9 minimal medium (standard). *Cold Spring Harbor Protocols* 2010, *2010* (8), .
(30) N-Dodecyl-N,N-dimethyl-3-ammonio-1-propanesulfonate. https://www.sigmaaldrich.com/catalog/product/sigma/d0431?lang=en&region=US.
(31) Philo, J. S. Improved methods for fitting sedimentation coefficient distributions derived by time-derivative techniques. *Anal. Biochem.* **2006**, *354* (2), 238−46.
(32) Stafford, W. F., 3rd Boundary analysis in sedimentation transport experiments: a procedure for obtaining sedimentation coefficient distributions using the time derivative of the concentration profile. *Anal. Biochem.* **1992**, *203* (2), 295−301.
(33) Schuck, P. Size-distribution analysis of macromolecules by sedimentation velocity ultracentrifugation and lamm equation modeling. *Biophys. J.* **2000**, *78* (3), 1606−19.
(34) Ebel, C. Sedimentation velocity to characterize surfactants and solubilized membrane proteins. *Methods* **2011**, *54* (1), 56−66.
(35) Brooks, B. R.; Brooks, C. L., 3rd; Mackerell, A. D., Jr.; Nilsson, L.; Petrella, R. J.; Roux, B.; Won, Y.; Archontis, G.; Bartels, C.; Boresch, S.; Caflisch, A.; Caves, L.; Cui, Q.; Dinner, A. R.; Feig, M.; Fischer, S.; Gao, J.; Hodoscek, M.; Im, W.; Kuczera, K.; Lazaridis, T.; Ma, J.; Ovchinnikov, V.; Paci, E.; Pastor, R. W.; Post, C. B.; Pu, J. Z.; Schaefer, M.; Tidor, B.; Venable, R. M.; Woodcock, H. L.; Wu, X.; Yang, W.; York, D. M.; Karplus, M. CHARMM: the biomolecular simulation program. *J. Comput. Chem.* **2009**, *30* (10), 1545−614.
(36) Cheng, X.; Jo, S.; Lee, H. S.; Klauda, J. B.; Im, W. CHARMM-GUI micelle builder for pure/mixed micelle and protein/micelle complex systems. *J. Chem. Inf. Model.* **2013**, *53* (8), 2171−80.
(37) Jo, S.; Kim, T.; Iyer, V. G.; Im, W. CHARMM-GUI: a web-based graphical user interface for CHARMM. *J. Comput. Chem.* **2008**, *29* (11), 1859−65.
(38) Lee, J.; Cheng, X.; Swails, J. M.; Yeom, M. S.; Eastman, P. K.; Lemkul, J. A.; Wei, S.; Buckner, J.; Jeong, J. C.; Qi, Y.; Jo, S.; Pande, V. S.; Case, D. A.; Brooks, C. L., 3rd; MacKerell, A. D., Jr.; Klauda, J. B.; Im, W. CHARMM-GUI Input Generator for NAMD, GROMACS, AMBER, OpenMM, and CHARMM/OpenMM Simulations Using the CHARMM36 Additive Force Field. *J. Chem. Theory Comput.* **2016**, *12* (1), 405−13.
(39) Phillips, J. C.; Braun, R.; Wang, W.; Gumbart, J.; Tajkhorshid, E.; Villa, E.; Chipot, C.; Skeel, R. D.; Kale, L.; Schulten, K. Scalable molecular dynamics with NAMD. *J. Comput. Chem.* **2005**, *26* (16), 1781−802.
(40) Huang, J.; MacKerell, A. D., Jr. CHARMM36 all-atom additive protein force field: validation based on comparison to NMR data. *J. Comput. Chem.* **2013**, *34* (25), 2135−2145.
(41) Ryckaert, J.-P.; Ciccotti, G.; Berendsen, H. J. C. Numerical integration of the cartesian equations of motion of a system with constraints: molecular dynamics of n-alkanes. *J. Comput. Phys.* **1977**, *23* (3), 327−341.
(42) York, D. M.; Darden, T. A.; Pedersen, L. G. The effect of long-range electrostatic interactions in simulations of macromolecular crystals: A comparison of the Ewald and truncated list methods. *J. Chem. Phys.* **1993**, *99* (10), 8345−8348.
(43) Fleming, P. J.; Fleming, K. G. HullRad: Fast Calculations of Folded and Disordered Protein and Nucleic Acid Hydrodynamic Properties. *Biophys. J.* **2018**, *114* (4), 856−869.

https://dx.doi.org/10.1021/jacs.0c00290
J. Am. Chem. Soc. 2020, 142, 6227−6235

(44) Schuck, P., Zhao, H., Brautigam, C., Ghirlando, R. *Basic Principles of Analytical Ultracentrifugation*. 1st ed. ed.; CRC Press: Boca Raton, 2016.
(45) Hyberts, S. G.; Takeuchi, K.; Wagner, G. Poisson-gap sampling and forward maximum entropy reconstruction for enhancing the resolution and sensitivity of protein NMR data. *J. Am. Chem. Soc.* **2010**, *132* (7), 2145−7.
(46) Delaglio, F.; Grzesiek, S.; Vuister, G. W.; Zhu, G.; Pfeifer, J.; Bax, A. NMRPipe: a multidimensional spectral processing system based on UNIX pipes. *J. Biomol. NMR* **1995**, *6* (3), 277−93.
(47) Sun, S.; Gill, M.; Li, Y.; Huang, M.; Byrd, R. A. Efficient and generalized processing of multidimensional NUS NMR data: the NESTA algorithm and comparison of regularization terms. *J. Biomol. NMR* **2015**, *62* (1), 105−117.
(48) Keller, R. *Optimizing the process of nuclear magnetic resonance spectrum analysis and computer aided resonance assignment*. Ph.D. Thesis, Swiss Federal Institute of Technology: Zurich, 2005.
(49) Bhattacharya, S.; Sukits, S. F.; MacLaughlin, K. L.; Lecomte, J. T. The tautomeric state of histidines in myoglobin. *Biophys. J.* **1997**, *73* (6), 3230−40.
(50) Englander, S. W.; Mayne, L.; Bai, Y.; Sosnick, T. R. Hydrogen exchange: the modern legacy of Linderstrom-Lang. *Protein Sci.* **1997**, *6* (5), 1101−9.
(51) Edison, A. S.; Weinhold, F.; Markley, J. L. Theoretical Studies of Protium/Deuterium Fractionation Factors and Cooperative Hydrogen Bonding in Peptides. *J. Am. Chem. Soc.* **1995**, *117* (38), 9619−9624.
(52) Lee, W.; Tonelli, M.; Markley, J. L. NMRFAM-SPARKY: enhanced software for biomolecular NMR spectroscopy. *Bioinformatics* **2015**, *31* (8), 1325−7.
(53) Connelly, G. P.; Bai, Y.; Jeng, M. F.; Englander, S. W. Isotope effects in peptide group hydrogen exchange. *Proteins: Struct., Funct., Genet.* **1993**, *17* (1), 87−92.
(54) Zhang, Y. Z. *Protein and peptide structure and interactions studied by hydrogen exchanger and NMR*. Ph.D. Thesis, University of Pennsylvania, 1995.
(55) Capponi, S.; Heyden, M.; Bondar, A. N.; Tobias, D. J.; White, S. H. Anomalous behavior of water inside the SecY translocon. *Proc. Natl. Acad. Sci. U. S. A.* **2015**, *112* (29), 9016−21.
(56) Wimley, W. C.; Hristova, K.; Ladokhin, A. S.; Silvestro, L.; Axelsen, P. H.; White, S. H. Folding of beta-sheet membrane proteins: a hydrophobic hexapeptide model. *J. Mol. Biol.* **1998**, *277* (5), 1091−110.
(57) Botos, I.; Noinaj, N.; Buchanan, S. K. Insertion of proteins and lipopolysaccharide into the bacterial outer membrane. *Philos. Trans. R. Soc., B* **2017**, *372* (1726), 20160224.
(58) Noinaj, N.; Kuszak, A. J.; Gumbart, J. C.; Lukacik, P.; Chang, H.; Easley, N. C.; Lithgow, T.; Buchanan, S. K. Structural insight into the biogenesis of beta-barrel membrane proteins. *Nature* **2013**, *501* (7467), 385−90.
(59) Dong, H.; Xiang, Q.; Gu, Y.; Wang, Z.; Paterson, N. G.; Stansfeld, P. J.; He, C.; Zhang, Y.; Wang, W.; Dong, C. Structural basis for outer membrane lipopolysaccharide insertion. *Nature* **2014**, *511* (7507), 52−6.
(60) Qiao, S.; Luo, Q.; Zhao, Y.; Zhang, X. C.; Huang, Y. Structural basis for lipopolysaccharide insertion in the bacterial outer membrane. *Nature* **2014**, *511* (7507), 108−11.
(61) Bamert, R. S.; Lundquist, K.; Hwang, H.; Webb, C. T.; Shiota, T.; Stubenrauch, C. J.; Belousoff, M. J.; Goode, R. J. A.; Schittenhelm, R. B.; Zimmerman, R.; Jung, M.; Gumbart, J. C.; Lithgow, T. Structural basis for substrate selection by the translocation and assembly module of the beta-barrel assembly machinery. *Mol. Microbiol.* **2017**, *106* (1), 142−156.
(62) Towns, J.; Cockerill, T.; Dahan, M.; Foster, I.; Gaither, K.; Grimshaw, A.; Hazlewood, V.; Lathrop, S.; Lifka, D.; Peterson, G. D.; Roskies, R.; Scott, J. R.; Scott, J. R. XSEDE: Accelerating Scientific Discovery. *Comput. Sci. Eng.* **2014**, *16* (5), 62−74.

https://dx.doi.org/10.1021/jacs.0c00290
J. Am. Chem. Soc. 2020, 142, 6227−6235